Title
EXPERIMENTAL STUDY OF Yb NUCLEI AT HIGH ANGULAR MOMENTUM

Author
Simon, R.S.

Publication Date
1977

Submitted to Nuclear Physics

LBL-5827
Preprint

EXPERIMENTAL STUDY OF Yb NUCLEI AT HIGH ANGULAR MOMENTUM

R. S. Simon, M. V. Banaschik, R. M. Diamond,
J. O. Newton, and F. S. Stephens

January 1977

Prepared for the U. S. Energy Research and
Development Administration under Contract W-7405-ENG-48

DISCLAIMER

EXPERIMENTAL STUDY OF Yb NUCLEI AT HIGH ANGULAR MOMENTUM*

R. S. Simon†, M. V. Banaschik††, R. M. Diamond,
J. O. Newton††† and F. S. Stephens

Nuclear Science Division
Lawrence Berkeley Laboratory
University of California
Berkeley, California 94720

ABSTRACT

Methods have been developed to study the continuum gamma-ray spectrum following heavy-ion compound-nucleus reactions. In the Yb nuclei studied these spectra were found to depend mainly on the input angular momentum, and not on the target-projectile system. The gross features of the spectra are a high-energy tail of ~ 4 transitions corresponding to the statistical cascade and a lower-energy bump composed of many unresolved collective E2 transitions. Several methods were devised to obtain moment-of-inertia values from the detailed features of this bump for angular momenta as high as 50 $\hbar$.

---

*This work was done with support from the U. S. Energy Research and Development Administration.

†Present address, Gesellschaft für Schwerionenforschung, Darmstadt, Germany.

††Present address, Gesellschaft für Reaktorsicherheit, Köln, Glokengasse 2, Germany.

†††Present address, The Australian National University, Canberra, A.C.T. 2600 Australia.

1. Introduction

In heavy-ion compound-nucleus reactions the projectile can bring in large amounts of angular momentum. But in order to produce very high-spin states in the evaporation residues two conditions have to be met: the compound system must not fission; and the evaporated particles must not carry off too much angular momentum. These two processes limit the maximum angular momentum observed so far in the residual nuclei to $\ell \lesssim 70$.

A schematic diagram of excitation energy vs. angular momentum for rare-earth products from an ^{40}Ar reaction is shown in fig. 1. The lower, approximately parabolic curve is the yrast line, so that there are no levels in these nuclei at energies below this. The heavy bar is an estimate of the energy and angular momentum for states populated in a 4n reaction[1]). Their energies are roughly a neutron binding energy above the yrast line, and their angular momenta are between those of the 5n channel below and the 3n channel above the 4n region. It is important to understand both limitations. A fifth neutron is not likely to be emitted from the populated area indicated in fig. 1 since this decay would lead into a region of low level density very near the yrast line or even be completely forbidden energetically. Similarly, a compound nucleus with more than about I = 40 in fig. 1 would probably not emit the fourth neutron. From nuclei with I less than about 20, on the other hand, a fifth neutron will be emitted as more and more states in the 5n product become energetically available. Thus, there is a fractionation of the initial angular momentum among the residual nuclei, with the highest ℓ-values going into the channels with the fewest particles evaporated. This fractionation should be stronger at high angular momentum

where the yrast line becomes rather steep, but it is expected to get washed out at low angular momentum where the yrast line becomes relatively flat.

The gamma-ray deexcitation of the populated region is predicted to proceed through three types of cascade[2]). One of these is a statistical cascade (I) consisting mainly of high-energy dipole transitions. This carries off some excitation energy, but very little angular momentum. The gamma-ray spectrum from this cascade is expected to decrease exponentially in intensity above $\sim$ 2 MeV. To carry off angular momentum, the decay proceeds by stretched E2 transitions through a number of collective bands roughly parallel to the yrast line. This is the collective cascade (II). Here the gamma transition energy will be determined by the effective moments of inertia in the collective bands. Using liquid-drop model estimate[3]), one expects transition energies between 1 and 1.5 MeV for nuclei in the rare-earth region. Since none of the individual bands is likely to collect sufficient population to be distinguished, the collective cascade should produce a low-energy continuous "bump" in the gamma-ray spectrum. There is no experimental evidence that the collective cascades are close to the yrast line and we do not distinguish whether the statistical or the collective cascade occurs first. Around I = 20 the yrast levels become those of the ground-state band and an energy gap develops between these levels and others of the same spin. At this point the population begins to shift into this particular band, producing individual transitions with sufficient intensity to be identified in the spectrum, that is, the discrete lines of cascade (III).

Thus in the gamma-ray spectrum from an evaporation residue in the mass region around A = 160 there are three discernible features: low-energy discrete lines ($\lesssim$ 0.8 MeV); an unresolved relatively low-energy bump ($\lesssim$ 1.5 MeV); and an unresolved high-energy exponential tail. To get information about states at high angular momentum it is necessary either to develop new techniques to isolate very weak transitions from this unresolved "continuum" or to devise statistical methods to investigate the continuum. It is this second approach, the statistical one, that we have chosen for the present study. Several related studies have been made of these continuum gamma rays[4-12], including some preliminary reports of the present work.

2. Experimental Technique and Results

We have used bombardments of 88 MeV ^{16}O on ^{150}Sm, 161 MeV and 185 MeV ^{40}Ar on $^{126,130}Te$ and 309 MeV and 334 MeV ^{86}Kr on $^{80,82}Se$ to produce Yb nuclei in a broad range of angular momenta up to the limit which these nuclei can hold. The compound system most completely studied was ^{166}Yb. Additional results were obtained for ^{168}Yb via the ^{86}Kr reaction on ^{82}Se and for ^{170}Yb via ^{40}Ar bombardment of ^{130}Te.

The energies of the ^{16}O and ^{40}Ar beams from the 88" cyclotron are known to better than 1 MeV. The ^{86}Kr energies at the SuperHILAC were measured to $\sim$ 1% accuracy by time-of-flight and monitored during the experiments by a solid-state detector.

Our experimental arrangement to study the continuum γ rays from the evaporation residues is shown schematically in fig. 2. The beam strikes a thin target on 0.025 mm lead backing. Target thicknesses are below 1 mg/cm^2 and introduce less than $\pm$4 MeV spread around the average beam energy. (We will refer to these averages rather than the full incident beam energies from now on). The lead backing stops recoils and projectiles without generating appreciable background radiation. The γ continuum is observed in three 7.5 $\times$ 7.5 cm NaI(Tl) detectors at 0°, 45°, and 90° with respect to the beam direction and 60 cm from the target. These detectors are gated by coincident pulses from a 10 cm^3 planar Ge detector at 225° and 5 cm from the target. The coincidence requirement with the Ge detector serves two purposes: (1) to obtain the continuum spectrum associated with an individual reaction channel by gating on the discrete γ lines from the corresponding evaporation residue, and (2) to provide a time signal to distinguish pulses

in the NaI detectors due to γ rays from those due to neutrons on the basis of the longer neutron flight times.

In order to illustrate the method of reaction channel selection, a Ge coincidence spectrum from the $^{126}Te + ^{40}Ar$ reaction at 181 MeV is shown in fig. 3. The discrete γ lines of ^{162}Yb and ^{161}Yb corresponding to the 4n and 5n channels can be readily identified. In the analysis of the data (stored event by event on magnetic tape) gates are set on the lines of interest, backgrounds are subtracted as determined from energy regions next to these lines, and then the sorted NaI spectra are summed for all lines from a given reaction channel since we have not found statistically significant differences between these spectra. Thus two (or three) channels from a reaction can be studied simultaneously, and due to the fractionation of the total angular momentum distribution they represent rather different average angular momenta.

The true energy distribution of the continuum γ radiation is obtained from the observed NaI pulse-height spectra by an "unfolding" procedure[4]) which assumes a distribution of Compton and pair production events for each full-energy γ quantum detected. To allow computer analysis, the detector response to γ radiation is represented by a two-dimensional matrix of experimental pulse-height distributions vs. γ-ray energies. Unfolding is achieved in successive steps: an initial guess of the true γ-ray energy distribution is multiplied by the response matrix to generate the corresponding pulse-height spectrum. This spectrum is compared to the experimental one and deviations between the two are used to improve the estimate for the next iteration. Two parameters of the carefully adjusted detector response are given in fig. 4

where the total absolute efficiency and the full-energy peak/total ratio are plotted as a function of incident γ-ray energy. It is the small peak/total ratio which considerably enhances the statistical fluctuations of the unfolded spectra. Multiple events, where more than one NaI detector fired at a given time, were suppressed electronically. Due to the high intrinsic γ-ray multiplicities of the reactions studied, such pile-up effects are not completely negligible even at 60 cm distance and require an overall correction to the unfolded spectra of somewhat less than 4%.

Comparison of unfolded spectra from the NaI detectors at 0° and 90° (after a small correction for the motion of the recoiling product nuclei) gives the anisotropy of the continuum γ rays. Calculations[13]) show that the beam-γ-γ correlation with the Ge detector at 225° is qualitatively similar to the usual beam-γ distribution; i.e. the $0^\circ/90^\circ$ ratio is about 1.4 for stretched quadrupole radiation and about 0.7 for stretched dipole transitions. The sum of the unfolded spectra from all three detectors gives a nearly isotropic spectrum. Decreased by about 3% and normalized to the number of single events in the gating lines of the Ge detector, this isotropic unfolded spectrum can be expressed in absolute events per decay and may be integrated to give the average γ-ray multiplicity, $\bar{N}_\gamma$, of the reaction.

For the reaction ^{126}Te (^{40}Ar, 4n) ^{162}Yb at 181 MeV the original, "raw" pulse-height spectrum and the unfolded spectrum are shown in fig. 5, as well as the ratio of events at 0° to those at 90°. To obtain $\bar{N}_\gamma$, we have summed the transitions in the unfolded spectrum above 0.34 MeV (the lowest energy considered to be reliable) and then

added two transitions to represent the 166-keV $2^+ \rightarrow 0^+$ and 320-keV $4^+ \rightarrow 2^+$ lines in ^{162}Yb. Another 0.25 of a transition corrects for the gates at 437 keV and 578 keV in the Ge detector in this case. The average γ-ray multiplicities for all the reactions studied are listed in table 1.

Absolute cross sections for the various xn reaction channels have been obtained from the Ge singles spectra in two ways. In the first method, the γ intensities of interest, corrected for pile-up, for the relative efficiency of the Ge detector, and for internal conversion, are compared to the corrected intensity of the 803 keV $2^+ \rightarrow 0^+$ transition in ^{206}Pb which is produced simultaneously by Coulomb excitation of the natural lead backing. The 803 keV γ-ray yield can be derived from semi-classically calculated populations[14,15]) of the 2^+ state, and the projectile stopping powers in lead, thus leading to an absolute normalization. The target thicknesses were determined by X-ray fluorescence. The other method compares the corrected γ intensities with the $2^+ \rightarrow 0^+$ Coulomb-excitation yield of the target measured at a safe bombarding energy below the barrier. Relative integrated beam intensities and electronic live times for the two runs are required to relate the calculated Coulomb-excitation cross sections to the desired xn cross sections.

For the Ar- and Kr-induced reactions the results from both methods agree, and averages are used for final values. The ^{150}Sm (^{16}O,xn) cross sections are those from comparison with Coulomb excitation of ^{150}Sm only, because the projectile energies in the fusion bombardments were above the Coulomb barrier for ^{206}Pb in part of the backing. The observed xn cross sections are given in table 1. In the

odd residues ^{161,163}Yb only the decoupled $i_{13/2}$ band transitions are known. To allow for other bands the measured $i_{13/2}$ band populations have been increased by 35%, the measured value in ^{175}Yb.

As an example, the γ-singles spectrum corresponding to the ^{126}Te + ^{40}Ar reaction at 181 MeV is shown in fig. 6. The xn lines clearly dominate the spectrum. Somewhat unfortunately the $8^+ \rightarrow 6^+$ transition in ^{162}Yb at 521 keV is contaminated by the $25/2^+ \rightarrow 21/2^+$ transition in ^{161}Yb at the same energy. Similarly the $4^+ \rightarrow 2^+$ transition in ^{160}Yb at 395 keV is not resolved from the $21/2^+ \rightarrow 17/2^+$ transition in ^{161}Yb at 396 keV. Besides the pure neutron evaporation residues, evidence is seen for αxn products from ^{160}Er (lines at 126 and 264 keV) down to ^{157}Er (266 and 415 keV). These αxn products can be identified in all reactions proceeding through the compound system ^{166}Yb. But while they correspond to about 8% of the total xn cross section in the other cases studied, their relative intensity is almost doubled in the 181 MeV ^{40}Ar spectrum shown in fig. 6. Alpha emission from the ^{168}Yb system is reduced as expected, and it seems to be negligible from the system ^{170}Yb.

The γ-decay from very high-spin isomers would offer a unique possibility to study discrete transitions between high-angular-momentum states. The decay of such an isomer should be characterized by the high multiplicity of the subsequent γ-ray cascade, and we have searched for the prompt γ-γ- coincidences between the beam bursts of the ^{130}Te + ^{40}Ar bombardment at 181 MeV. The beam repetition rate of the cyclotron was 6.5 MHz and a γ-beam time-resolution better than 8 ns was maintained over the 30 hours of the experiment. Thus our arrangement

was sensitive to isomeric lifetimes from ∿ 10 ns to ∿ 10 days (this covers about one third of the full logarithmic time-scale from nuclear times to the age of the universe).

The out-of-beam Ge-detector spectrum in coincidence with any of the NaI detectors is shown in the upper part of fig. 7 and can be compared with the corresponding in-beam spectrum below. None of the prominent xn lines can be safely identified in the out-of-beam spectrum. From this we estimate that less than 0.1% of the total population of these these xn-channels is delayed in high-spin traps with lifetimes between $10^{-9} \leq \tau \leq 10^{6}$s. Recent theoretical calculations[16,17]) also suggest that high spin traps might not be very common.

3. Discussion

The shapes of the continuum spectra and their normalized intensities represent our primary information on the high-spin states of the nuclei studied. These results will be combined with estimates of the angular momentum carried off by the γ decay to derive effective moments of inertia for these Yb nuclei for angular momenta up to $\ell = 50$.

3.1 GROSS STRUCTURE OF CONTINUUM SPECTRA

The unfolded spectra have a common general structure. Their intensity decreases nearly exponentially with energy at high γ energies, and somewhere below 1.5 MeV they show a rather pronounced "bump" of intensity rising from this exponential tail. This feature is clearly seen in the spectrum of ^{162}Yb from the ^{40}Ar, 4n reaction at 181 MeV given in fig. 5 and is present even in the original raw spectrum.

The exponential tail above 1.5 MeV seems to have no sharp high-energy cut-off and has a slope which is consistent with estimates for a statistical cascade[1]). The nearly isotropic angular distribution in the tail region is also consistent with this conclusion, as is the general similarity of this part of the spectrum in the various reactions studied. From this, and from previous work[8,10]), it is very likely that these transitions do come, at least mainly, from the predicted statistical cascade.

Below about 1.5 MeV, in the bump region, the anisotropy suggests a dominance of stretched-E2 $I \rightarrow I-2$ transitions. Here the spectrum does change with bombarding conditions. At the bottom of fig. 5 the shape of the unfolded ^{162}Yb spectrum from the ^{40}Ar,4n reaction at 181 MeV (obtained from the spectrum above) is compared with that from the

same 4n reaction channel at 157 MeV and with spectra from the ^{150}Sm (^{16}O, 4n) and ^{80}Se (^{86}Kr, 4n) reactions. The last three bombardments, though very different in their target-projectile combinations, generate almost identical spectra. Very clearly, the bump in the 181 MeV ^{40}Ar spectrum is more developed and extends to higher energies. This seems to be an angular-momentum effect and suggests that the bump arises from the predicted collective transitions parallel to the yrast line. It is natural then to expect similar spectra from the ^{16}O and the low-energy ^{40}Ar and ^{86}Kr reactions shown, since similar amounts of angular momentum are brought into the compound system in these cases. Increasing the angular-momentum input, as in the 181 MeV ^{40}Ar reaction, extends the collective cascade to higher energies. In fig. 8 the 4n shapes are compared with schematic spectra from odd-n reaction channels. The important point is that the portion of the bump above $\sim$ 0.8 MeV seems to depend mostly on the angular-momentum input and very little on the final nucleus. The 5n-channel from the 181 MeV ^{40}Ar reaction looks very much like the 4n-channel in the 157 MeV ^{40}Ar data (and like the ^{16}O and ^{86}Kr spectra). This is consistent with the expected fractionation of the total angular momentum which predicts about the same average spins for these two channels. Similarly, the 3n reaction at 157 MeV resembles the 4n reaction at 181 MeV, but the statistics for this 3n reaction are rather poor.

It is reasonably convincing from these spectra that there exists an edge, or upper energy limit for the bump, and in cases of adequate statistics we have read off these edge energies. They are listed in Table 1.

3.2 MULTIPLICITIES AND ANGULAR MOMENTA

In table 1 are listed the average multiplicities, $\bar{N}_\gamma$, for the different reaction channels studied in this work. Several trends are clear. For a given reaction channel, i.e., 3n, 4n, 5n or 6n, the value of $\bar{N}_\gamma$ increases with the bombarding energy of the projectile, indicating that the length of the yrast cascade increases when more angular momentum is brought into the compound nucleus. In addition, it can be seen that the value of $\bar{N}_\gamma$ is larger, the smaller the number of neutrons emitted from a particular compound system, again suggesting a longer yrast cascade for higher angular momenta. To relate $\bar{N}_\gamma$ to the average channel angular momentum we estimated these angular momenta from the measured channel cross sections using the sharp cut-off model[18]).

Within the framework of this model the maximum angular momentum possible in a collision is:

$$\ell_{max} = \frac{R}{\hbar}\sqrt{2\mu(E-V)} \quad , \tag{1}$$

where R is the sum of the radii of target and projectile nucleus, μ is the reduced mass of the system, and E and V are the kinetic energy and the Coulomb barrier in the center of mass coordinate frame. The sum of the radii R we calculate from the mass numbers A of the particles according to[19]):

$$R = 1.16 \left(A_{proj.}^{1/3} + A_{targ}^{1/3} + 2 \quad fm\right) \quad , \tag{2}$$

and the Coulomb barrier V from the atomic numbers Z according to:

$$V = \frac{1.44\ Z_{proj} \cdot Z_{target}}{R}\ \text{MeV} \qquad (3)$$

The contribution of a partial ℓ wave of the incoming beam to the total fusion cross section is given by

$$\sigma_\ell = \pi\ \lambda^2(2\ell+1) \qquad (4)$$

where $0 \leq \ell \leq \ell_{max}$ and λ is the de Broglie wavelength of the projectile.

To relate the angular momentum in a particular reaction channel to its partial cross section, we have assumed that the total angular momentum distribution is fractionated into sharp bins for each reaction product. (We have pointed out earlier that there is fractionation, but it is probably not very sharp.) With this assumption, the cross section for a particular reaction channel is a summation of partial waves between a lower and an upper angular momentum limit, the edges of its bin,

$$\Delta\sigma = \sum_{\ell_e}^{\ell_u} \sigma_\ell = \pi\lambda^2[\ell_u(\ell_u+1) - \ell_\ell(\ell_\ell+1)] \quad . \qquad (5)$$

This sum may be identified with the experimental value for the cross section of the particular xn channel. Thus, for example, with 181 MeV ^{40}Ar on ^{126}Te, the 6n population would fall into the lowest bin starting with angular momentum $\ell = 0$, and the 5n, 4n and 3n channels would follow in that order. With $\pi\lambda^2 = 0.157$ mbarn for this reaction, we determine the 6n-5n boundary to be $\ell_u(6n) = 20$. The next two boundaries are $\ell_u(5n) = 46$ and $\ell_u(4n) = 62$ and, including the 3n channel, gives

ℓ_{max} (xn) = 64. These numbers include contribution to each cross section due to charged particle channels competing with the nx channels, about 8% of the xn cross section in αxn channels (measured) and an equal amount in pxn channels (estimated). The value of ℓ_{max}(xn) is smaller than the maximum angular momentum ℓ_{max} = 74 calculated from eq. 1; however, fission of the compound nucleus or emission of α particles which compete with γ decay by carrying angular momentum would reduce the limit. It seems likely to us that both fission and α emission are important in these Yb nuclei and the increased cross section of the αxn channels in the ^{126}Te + ^{40}Ar reaction at 181 MeV might indicate this. Unlike the contribution of ∿ 8%, seen from the ^{166}Yb systems produced at any lower angular momentum, the increase at 181 MeV would then correspond to α emission from the top of the angular-momentum distribution. Thus the additional 8% was not added in as parallel to the xn channels.

In the ^{150}Sm + ^{16}O reaction (and in several other cases) an odd-n channel is lowest in angular momentum, and population falling into the slice from ℓ = 0 to ℓ = 13/2 (the spin of the decoupled $i_{13/2}$ band head) will be missing from the experimental channel cross section in table 1. In the ^{150}Sm + ^{16}O reaction this amounts to about 10% of the 5n cross section as estimated from the sharp cut-off model and is added to the experimental value before calculating ℓ_u(5n).

Average angular momenta for the individual channels are obtained from the upper and lower limits according to:

$$\bar{\ell}(\sigma) = \frac{2}{3} \frac{\ell^3_{upper} - \ell^3_{lower}}{\ell^2_{upper} - \ell^2_{lower}} \quad . \qquad (6)$$

These average values are compared with the corresponding average γ-ray multiplicities in fig. 9 after the odd-n channel multiplicities have been increased by 3 to treat them on the same footing as the even-n values (the prompt cascade down the decoupled $i_{13/2}$ band leaves the odd nuclei with 13/2 units of angular momentum which would correspond to about 3 more γ transitions).

A relationship between the average γ-ray multiplicity $\bar{N}_\gamma$ and the average channel angular momentum $\bar{\ell}(\sigma)$ as derived from the cross sections is clearly established in fig. 9. The average ratio of $\bar{\ell}(\sigma)/\bar{N}_\gamma$ is close to 2, very much in agreement with the E2-character of the bump. There are no obvious differences between the ^{16}O, ^{40}Ar and ^{86}Kr points. Thus, the $\bar{N}_\gamma$ values observed seem to be generally consistent with a picture where the total angular momentum distribution is fractionated on the individual xn channels. The situation might be different for lighter ions, where less angular momentum is brought into the compound system, and the slope of the yrast line is correspondingly smaller.

The fact that there are no trends found distinguishing the ^{16}O, ^{40}Ar and ^{86}Kr points leads to an additional conclusion, namely that the same angular momentum range is involved for each projectile. This result is in disagreement with the suggestion that there is a lower critical angular momentum (as well as an upper one) for compound nucleus formation using Kr particles, in contrast to the situation with ^{40}Ar- and ^{16}O-induced reactions where compound nucleus formation starts at $\ell = 0$. That is, it has been proposed that Kr collisions involving impact parameters corresponding to $0 \leq \ell \leq 45$ lead to deep

inelastic scattering rather than compound nucleus formation, and the latter occurs only for $\ell > 45$. This proposal was a possible explanation for the narrower Kr excitation functions compared to the corresponding ^{40}Ar ones, and also for the marked shift in the threshold energy. We can offer no alternative explanation for those experimental results, but believe the idea of a lower angular momentum cut-off is incompatible with the present results.

The data in fig. 9 provide an empirical relationship between the average γ-ray multiplicity, $\overline{N}_\gamma$, and the average angular momentum of the original compound system. We have fitted a straight line to the points. If the statistical γ-rays carry off no angular momentum, as seems probable at low total angular momentum, then the intercept on the $\overline{N}_\gamma$ axis should indicate their number. The observed value of 4 is in good agreement with the intensity of the statistical cascade as estimated from the exponential tail in the unfolded spectra plus an estimated statistical background from underneath the yrast bump. The slope of the line in fig. 9 is 0.43, corresponding to $\Delta\ell = 2.3$ per collective transition. Octupole transitions are ruled out because of their lifetimes, so the transitions must be almost entirely collective stretched-E2 γ-rays. The increase above $\Delta\ell = 2$ has several causes. One important reason is that the evaporated neutrons, and possibly the statistical γ-cascade, carry off angular momentum. It seems plausible to us that the amount so carried should be proportional to the total angular momentum. A reduction of the initial angular momentum of the compound system by $\sim$ 15% to allow for the neutrons seems to fit the data. In addition, the value of the average angular momentum

has been calculated from the cross section by assuming that one reaction channel takes a certain angular-momentum range and then closes as the next channel opens in the next angular-momentum range. Since the reaction channels are almost certainly not that distinctly fractionated in angular-momentum, there is likely to be some overlap. If so, the average value for a reaction channel in a high-spin range will be lower than has been calculated, and that for a reaction channel in a low-angular-momentum range will be higher than has been calculated. The high- and low-spin points do deviate slightly in just this manner.

It seems clear that there is a correlation between the average γ-ray multiplicity and the average value of the angular momentum in the original compound system, and that the correlation should be even better between the multiplicity, $\overline{N}_\gamma$, and the average value of the angular momentum, $\overline{\ell}$, at the start of the γ-ray cascade after particle emission. The value of $\overline{\ell}$ is approximately $2\overline{N}_\gamma$, or more accurately $2(\overline{N}_\gamma - \delta)$, where δ accounts for the γ-rays carrying no angular momentum, and is around 4 in the present case. If such a relationship between $\overline{N}_\gamma$ and $\overline{\ell}$ proves general (and it has been obtained in other multiplicity studies) then it becomes an important and useful method to obtain the average angular momentum left in a particular reaction product at the start of the γ-cascade, as the average γ-ray multiplicity is a quantity readily determined. The N_γ values will be used for this purpose in the next section.

3.3 EFFECTIVE MOMENTS OF INERTIA

In the ground-state rotational bands of these rare-earth nuclei moments of inertia $\mathcal{I}$ have been calculated using the approximate relation,

$$E_t = \frac{\hbar^2}{2\mathcal{I}}(4I-2), \tag{7}$$

which connects an E2 transition energy E_t with the spin I of the decaying state. In fig. 10 we show the usual backbending type of plot for ^{162}Yb, where $2\mathcal{I}/\hbar^2$ is plotted against $(\hbar\omega)^2$, the square of the rotational frequency (which is very nearly $E_t^2/4$). Around spin 12 the moment of inertia rises sharply, suggesting that the curve will backbend as it does in the isotone ^{160}Er. It is interesting to look at that energy region in the unfolded spectra produced via the ^{166}Yb compound system (figs. 5 and 8). There is structure in the spectra of the 4n reactions around 0.5 MeV which is totally missing in the 3n and 5 n cases, and this very likely corresponds to the expected backbend in ^{162}Yb. On the other hand, the most heavily populated odd-mass bands are expected to behave regularly in this energy region and apparently do so. This is a rather direct illustration of the kind of information contained in these unfolded spectra.

The same relationship (7) can also be applied to high-spin states in the collective cascade, if we confine ourselves to a region of the spectrum corresponding to I values below which there is no appreciable direct population into the channel of interest. This region is likely to be below I = 35 for the 4n channel in the ^{126}Te + ^{40}Ar case at 181 MeV since most of the population with lower spins goes

into the 5n or 6n channels, but it would be less than I = 20 for the $^{16}0$ and low-energy Ar cases. Provided there is a monotonic increase of transition energy with spin (no additional backbending), a spin value for each transition energy can be obtained by summing all the transitions (less the estimated statistical-cascade background) up to that transition energy and multiplying by 2. This method is applicable between $\sim$ 0.7 and 1.0 MeV in the spectrum. The analysis can be followed in table 2 and leads to the moments of inertia given by the dots connected by a solid line in fig. 10.

It would be nice to follow the moment of inertia in this manner all the way up to the edge of the bump at 1.4 MeV. To do so requires additional information on the feeding pattern into the 4n channel, which we do not have at the present time. However, the necessary data could be obtained from experiments measuring the higher moments of the γ-ray number distribution. (The corresponding additional information would allow us to analyze the $^{16}0$, low-energy ^{40}Ar and ^{86}Kr cases, too).

Another place in the spectra where relation (7) may give moments of inertia is at the edge of the bump. From the bottom part of fig. 5 the edge in the ^{40}Ar spectrum at 181 MeV is clearly higher than in the other three cases where less angular momentum is brought into the system. This suggests that the energies of the edge (given in table 1) can be associated with γ-transitions between the highest spin states in the collective cascade. On the basis of this assumption, four values for $2\mathcal{J}/\hbar^2$ can be obtained and are plotted in fig. 10. As an estimate of the angular momentum at the top of the collective cascade we used the corresponding upper channel angular momentum as derived

from the cross sections, but subtracted 15% to allow for the amount carried off by neutrons and the statistical cascade. During a back-bend the edge of the bump and the top γ-transition energy in the cascade would not be identical and then moments of inertia would not be derivable in this manner.

The preceding method is an "integral" one and thus not very sensitive to local variations in the moment of inertia. There exists an alternative, a "differential" method, that can show such local variations. Each point on the unfolded spectrum of fig. 1 gives the number of transitions per 0.04 MeV energy interval ($\bar{N}_\gamma$ in table 2). The reciprocal of this ($.04/\bar{N}_\gamma$) is the difference between transition energies ΔE_t and can be related to the moment of inertia by differentiating express (7) for E_t, yielding

$$\Delta E_t = \frac{8\hbar^2}{2\mathcal{J}} - \frac{2E_t \, d\ell n \mathcal{J}}{dI} \qquad (8)$$

This method also requires the full population in the channel, and thus again can only be applied quantitatively below I = 35 in the 181 MeV ^{40}Ar case. For the region between 0.7 and 1.0 MeV, $\mathcal{J}$ is nearly constant so that the last term of eq. (8) can be neglected, giving $2\mathcal{J}/\hbar^2 \approx 8/\Delta E_t$. This procedure may be followed in table 2 and leads to the diamonds connected by the dashed line in fig. 10. The results are in good agreement with those from the integral method and this agreement suggests that the various approximations used are reasonable. The power of the differential method is that changes in the moment of inertia can be recognized directly from irregularities in the spectrum,

thereby providing a simple means to pick out regions of particular interest, namely, regions showing some type of structure.

The effective moments of inertia measured by the techniques described above are compared in fig. 10 with that of a rigid diffuse sphere of mass 162, having an equivalent rms radius[21]) of 6.71 fm. The deformed rigid-body value for the moment of inertia would be roughly 10% larger than this rigid-sphere value. The data above spin $20 - (\hbar\omega)^2 \sim 0.12$ MeV^2 – are nearly consistent with the rigid sphere estimate, but seem likely to be below the deformed value at least up to spin $40 - (\hbar\omega)^2 \sim 0.35$ MeV^2). Since 162 Yb is almost certainly deformed, this might indicate that there are still some pairing correlations (or other effects) at these spin values which reduce the effective moment of inertia below the rigid-body value.

4. Conclusion

We have developed methods to study the γ-ray continuum spectra from Yb evaporation residues produced by various heavy-ion reactions. These spectra clearly have a gross structure with two components. One is a high-energy exponential tail which we associate with a statistical cascade of $\sim$ 4 transitions. The other is a lower energy bump of stretched E2 transitions that correspond to the many collective rotational bands that cascade down parallel to the yrast line.

Since most of the γ-rays are in the yrast bump, it has been shown that a fairly good estimate of the average angular momentum carried by the γ-ray cascade in a particular reaction channel can be obtained by multiplying the average γ-ray multiplicity determined for that channel, $\bar{N}_\gamma$, by two, and that still better values can be obtained with certain small corrections. Furthermore, no observable difference was found among different reactions (target-projectile combinations) in the relationship between $\bar{N}_\gamma$ and the angular momentum involved at the start of the neutron cascade, as determined from the cross sections using the sharp cut-off approximation. (This result is in disagreement with the idea of a lower critical angular momentum for compound nucleus formation with Kr projectiles.) In all of the reactions studied, however, there was considerable fractionation of the angular momentum depending on the product nucleus.

We have shown that there is a relationship between the maximum energy of the bump and the angular momentum input. The form of the bump is well represented by assuming that the γ-rays cascade down collective rotational bands characterized by an average moment of

inertia which increases towards the rigid-body value at high spin. To obtain effective moments of inertia at these high spins, methods have been developed to analyze the γ continuum above the discrete ground-state-band transitions. These methods have given the first values for effective moments of inertia in these nuclei at about spin 50. It will obviously be of interest to improve the methods in order to see more details of these moments of inertia and to extend the measurements to other nuclei.

Acknowledgments

We are indebted to Drs. I Ragnarsson, D. P. Soroka, and W. J. Swiatechi for numerous discussions of nuclei at high angular momenta. We are also indebted to the operating crews of the 88" cyclotron and the SuperHILAC for providing the beams used in these studies.

References

1) J. R. Grover and J. Gilat, Phys. Rev. 157 (1967) 814.

2) J. O. Newton, F. S. Stephens, R. M. Diamond, W. H. Kelly, and D. Ward, Nucl. Phys. A141 (1970) 631.

3) S. Cohen, F. Plasil and W. J. Swiatecki, Ann. of Phys. (New York) 84 (1974) 1.

4) J. F. Mollenauer, Phys. Rev. 127 (1962) 867.

5) Yu. Ts. Oganesyan, Yu. V. Lobanov, B. N. Markov, and G. N. Flerov, Soviet Phys. JETP 17 (1963) 791.

6) P. Tjøm, F. S. Stephens, R. M. Diamond, J. de Boer, and W. E. Meyerhof, Phys. Rev. Letters 33 (1974) 593.

7) E. der Mateosian, O. C. Kistner, and A. W. Sunyar, Phys. Rev. Letters 33 (1974) 596.

8) J. O. Newton, J. C. Lisle, G. D. Dracoulis, J. R. Leigh, and D. C. Weisser, Phys. Rev. Letters 34 (1975) 99.

9) M. Fenzl and O.W.B. Schult, Z. Physik 272 (1975) 207.

10) M. V. Banaschik, R. S. Simon, P. Colombani, D. P. Soroka, F. S. Stephens, and R. M. Diamond, Phys. Rev. Letters 34 (1975) 892.

11) G. B. Hagemann, R. Broda, B. Herskind, M. Ishihara, S. Ogaza, and H. Ryde, Nucl. Phys. A245 (1975) 166.

12) R. S. Simon, M. V. Banaschik, P. Colombani, D. P. Soroka, F. S. Stephens and R. M. Diamond, Phys. Rev. Letters 36 (1976) 359.

13) Based on the computer code given by K. S. Krane and R. M. Steffen, Los Alamos Scientific Laboratory, report LA-4777, UC-34.

14) A. Winther and J. de Boer, California Institute of Technology report, Nov. 18, 1965.

15) J. L. Quebert, K. Nakai, R. M. Diamond, and F. S. Stephens, Nucl. Phys. A150 (1970) 68.

16) A. Faessler, M. Ploszajzyak, and K.R.S. Devi, Phys. Rev. Letters 36 (1976) 1028.

17) G. Andersson, S. E. Larsson, G. Leander, P. Möller, S. G. Nilsson, I. Ragnarsson, S. Åberg, R. Bengtsson, J. Dudek, B. Nerlo-Pomorska, K. Pomorski, and Z. Szymanski, preprint 1976.

18) J. M. Blatt and V. F. Weisskopf, Theoretical Nuclear Physics (John Wiley and Sons, New York, 1952).

19) W. J. Swiatecki, private communication (1967).

20) M. Lefort, Phys. Rev. C12 (1975) 686.

21) W. D. Meyers, Nucl. Phys. A204, (1973) 465.

Table 1. Data on Yb evaporation residues

Reaction		a) (mbarn)	b) ℓ_u	$\overline{\ell}(\sigma)$	$\overline{N}_\gamma$	$\overline{\ell}(\gamma)$	E_{edge}(MeV)
$^{150}Sm(^{16}O,3n)$		35±7	39±2	39±2	17±2	33±4	1.09±0.08
87 MeV	4n	495±50	38±2	30±2	17±1	26±3	1.12±0.05
	5n	193±20	21±1	15±1	8±1	15±3	0.88±0.08
$^{126}Te(^{40}Ar,3n)$		85±15	47±2	44±2	20±2	39±5	1.36±0.06
157 MeV	4n	219±22	41±2	30±2	17±1	26±3	1.16±0.05
	5n	34±7	16±2	12±1	8±2	15±4	
$^{126}Te(^{40}Ar,3n)$		28±5	64±4	63±4	26±2	44±5	
181 MeV	4n	239±24	62±4	54±4	24±2	40±5	1.40±0.05
	5n	238±40	46±3	35±3	15±1	29±3	0.96±0.08
	6n	53±6	20±1	14±1	9±1	10±2	
$^{80}Se(^{86}Kr,$ 2n)		33±5	44±4	42±4	22±3	36±5	
306 MeV	3n	110±17	40±3	31±2	12±2	23±4	
	4n	36±6	20±2	13±2	8±2	8±4	
$^{80}Se(^{86}Kr,$ 3n)		125±20	61±5	54±4	23±2	44±5	
331 MeV	4n	166±25	47±4	35±3	18±2	28±4	1.20±0.06
	5n	24±5	18±2	14±2			
$^{82}Se(^{86}Kr,$ 2n)		20±5	42±4	41±4	24±3	40±6	
306 MeV	3n	90±18	40±4	33±3	15±2	29±3	
	4n	62±12	25±3	17±2	12±2	16±3	
$^{82}Se(^{86}Kr,$ 3n)		77±15	53±4	49±4	24±2	47±5	
331 MeV	4n	116±23	44±3	35±3	20±2	31±3	
	5n	51±10	25±2	18±2	6±2	11±4	
$^{130}Te(^{40}Ar,4n)$		100±10	61±3	58±3	28±2	48±4	1.52±0.05
181 MeV	5n	260±26	55±3	47±3	21±1	41±3	1.42±0.06
	6n	188±19	37±3	27±2	16±1	24±2	
	7n	18±4	13±2	10±2			

a) for ^{161}Yb and ^{163}Yb the measured decoupled $i_{13/2}$ band population was increased by 35% to allow for other bands.

b) includes 15% of xn cross section for charged particle evaporation from ^{166}Yb compound system and 8% from ^{168}Yb system.

Table 2. Moments of inertia in ^{162}Yb evaluated from the γ continuum between 0.7 and 1 MeV.

Channel number [a]	E_t keV	$(\hbar\omega)^2$ $(MeV)^2$	$\bar{n}_\gamma$	$\sum \bar{n}_\gamma$	I	$\frac{4I-2}{E_t}$ MeV^{-1}	$\frac{8}{\Delta E_t}$ [b] MeV^{-1}
17	680	0.116	0.63	10.73	21.5	124	
18	720	0.130	0.77	11.50	23.0	125	134
19	760	0.144	0.57	12.07	24.1	124	
20	800	0.160	0.69	12.76	25.5	125	125
21	840	0.176	0.56	13.32	26.6	124	
22	880	0.194	0.76	14.08	28.2	126	155
23	920	0.212	0.79	14.87	29.7	129	
24	960	0.230	0.71	15.58	31.2	128	129
25	1000	0.250	0.58	16.16	32.3	127	

a) Refers to the normalized unfolded spectrum in fig. 5; $\bar{n}_\gamma$ gives the collective intensity per channel.

b) 2-channel averages starting with channel 18.

Figure Captions

Fig. 1 Energy and angular-momentum range of a rare-earth nucleus populated in an (^{40}Ar,4n) reaction. The proposed γ cascade pathway to the ground state is shown.

Fig. 2 Experimental arrangement to study continuum γ rays.

Fig. 3 Ge detector spectrum from the ^{126}Te + ^{40}Ar reaction at 181 MeV in prompt coincidence with one of the NaI detectors. The Ge coincidence spectra are used for setting gates to select the individual reaction channels.

Fig. 4 Response parameters of the NaI detectors for an absorber of 3.6 g/cm^2 Pb plus 2.8 g/cm^2 Cu. The experimental points correspond to transitions of 0.344 MeV from ^{152}Eu, 0.570 MeV from ^{207}Bi, 1.17 MeV from ^{60}Co, and 2.75 MeV from ^{24}Na. The smooth lines are based on results from calculations by R. L. Heath.

Fig. 5 Raw (□) and normalized unfolded (●) continuum γ spectrum from the reaction ^{126}Te(^{40}Ar,4n)^{162}Yb at 181 MeV. The larger dots represent 5-channel averages. Also shown is the 0/90 ratio for the true γ distribution. At the bottom are schematic spectra for this case (solid line) and for the reactions ^{80}Se(^{86}Kr,4n)^{162}Yb at 331 MeV (dotted line), ^{126}Te(^{40}Ar,4n)^{162}Yb at 157 MeV (longer-dashed line), and ^{150}Sm(^{16}O,4n)^{162}Yb at 87 MeV (shorter-dashed line).

Fig. 6 Ge detector singles spectrum from the ^{126}Te + ^{40}Ar reaction at 181 MeV. Absolute cross sections for the individual reaction channels are obtained from the singles spectra.

Fig. 7 Ge detector spectra from the $^{130}Te + ^{40}Ar$ reaction at 181 MeV in coincidence with any of the NaI detectors. The lower spectrum corresponds to events in the beam pulse of the cyclotron, the upper spectrum to coincidences in the time interval between 20 ns and 40 ns after the beam pulse.

Fig. 8 Schematic representation of Yb continuum spectra following ^{40}Ar reactions. The 5n and 4n channel at 181 MeV correspond to similar angular momenta as the 4n and 3n channel at 157 MeV.

Fig. 9 This figure plots the observed average γ multiplicities given in Table 1 against the average angular-momentum in that channel, also given in Table 1. Diamonds (♦), triangles (▲) and dots (●) indicate O, Ar and Kr results. The straight line fitted to the data has a slope of 0.43.

Fig. 10 Backbending plot for ^{162}Yb. The small dots indicate the known low-spin states whereas the open circles are for the isotone ^{160}Er. The large dots connected by a solid line correspond to ^{162}Yb values derived by the integral method from the 181 MeV ^{40}Ar spectrum between 0.7 and 1 MeV and the diamonds come from the differential method applied to the same data. The isolated square, triangles, and solid dot represent values from the top of the collective cascade as observed in the 87 MeV ^{16}O, 157 MeV ^{40}Ar, 331 MeV ^{86}Kr, and 181 MeV ^{40}Ar reactions. The horizontal dashed line corresponds to a rigid diffuse sphere with A = 162.

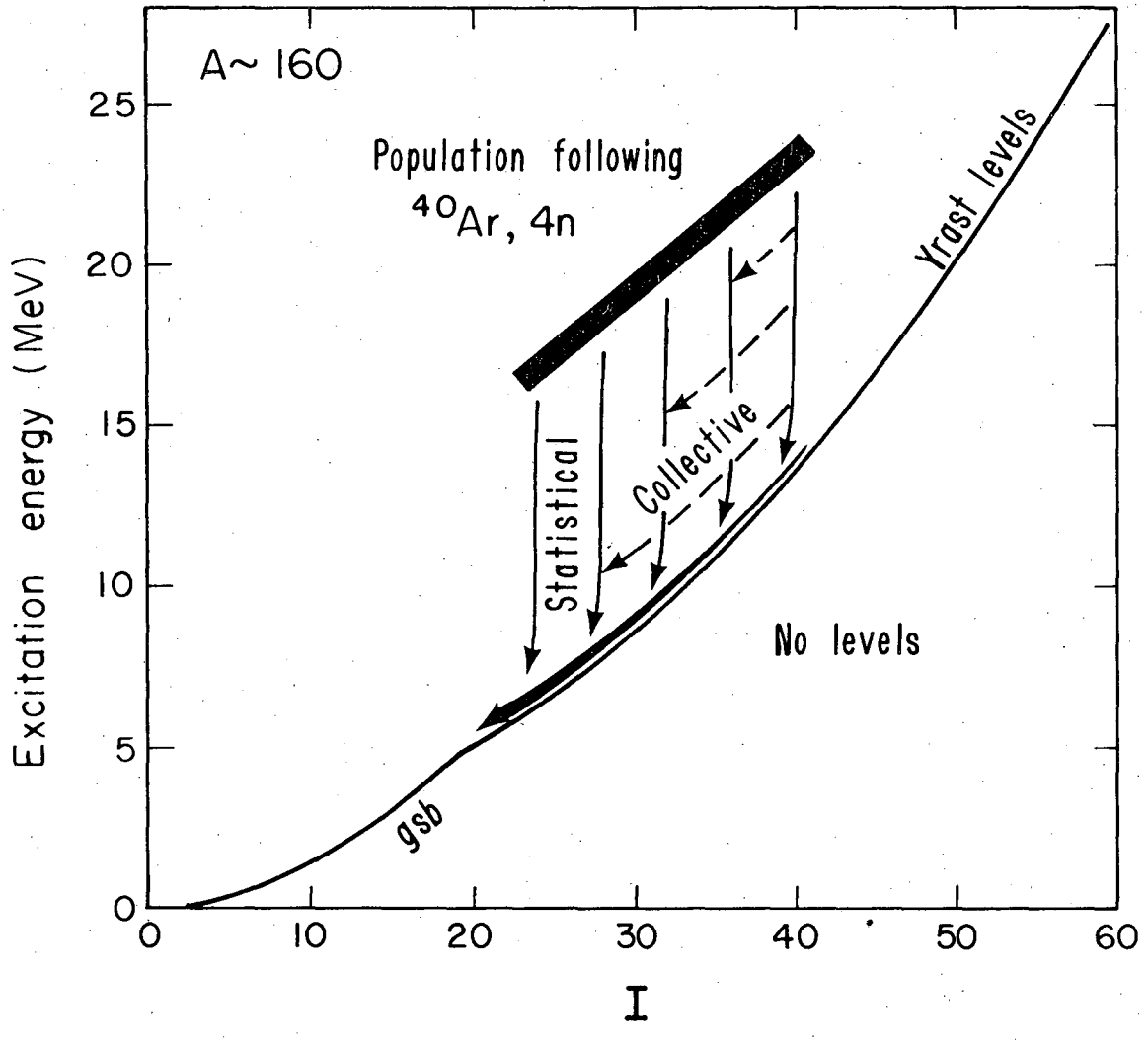

XBL 771-156

Fig. 1

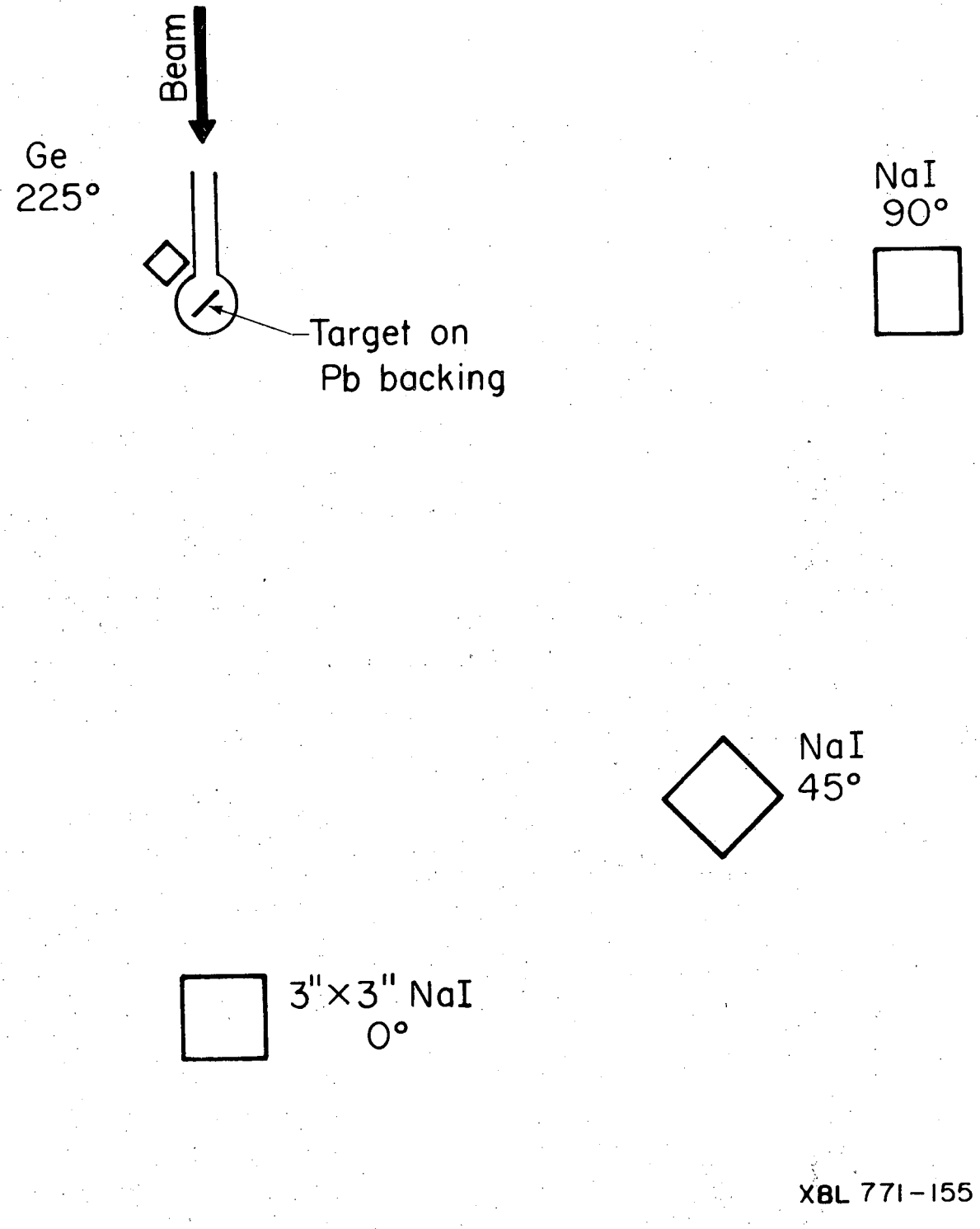
Beam
Ge
225°
Target on
Pb backing
NaI
90°
NaI
45°
3"×3" NaI
0°
XBL 771-155

Fig. 2

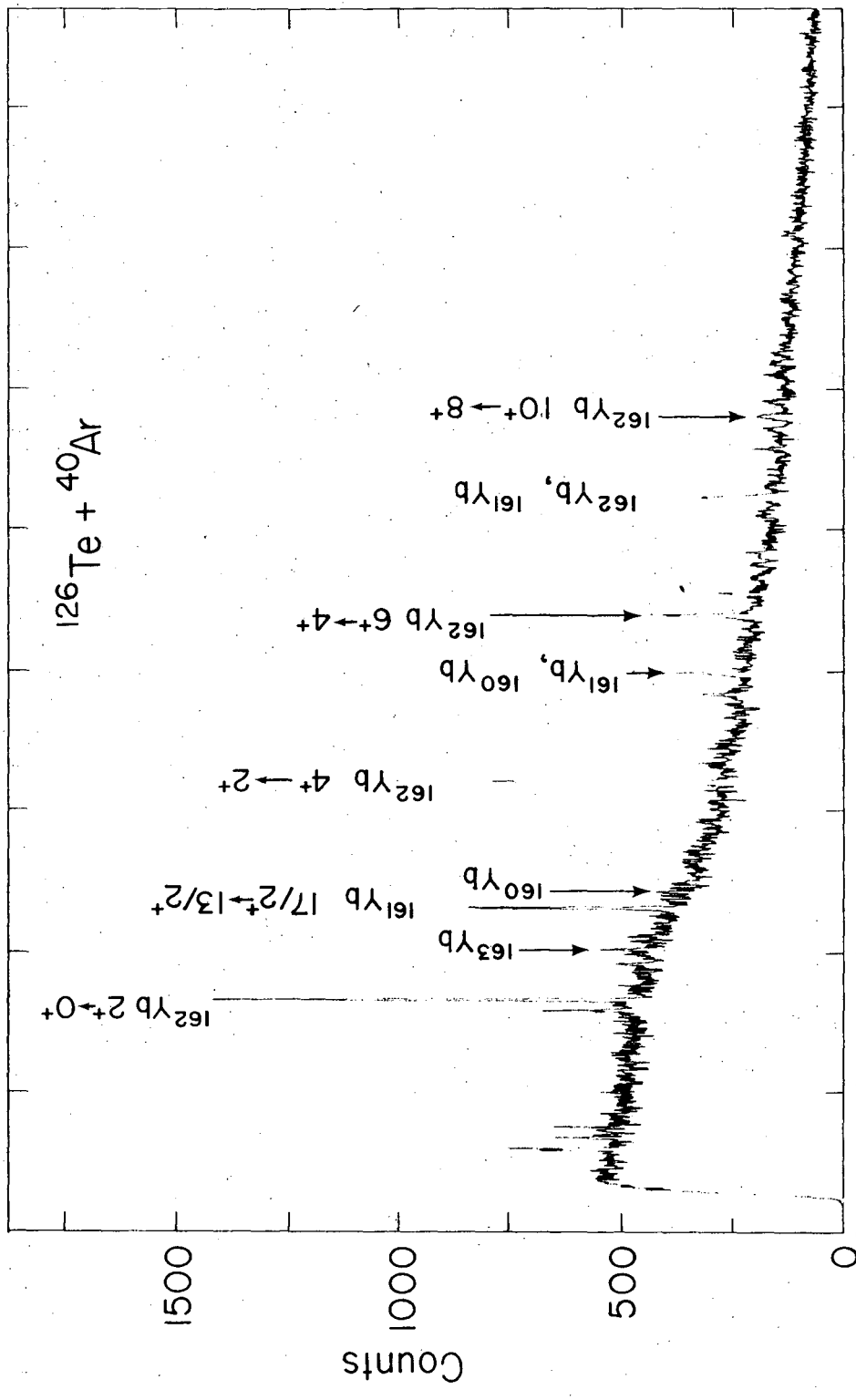

XBL 771-164

Fig. 3

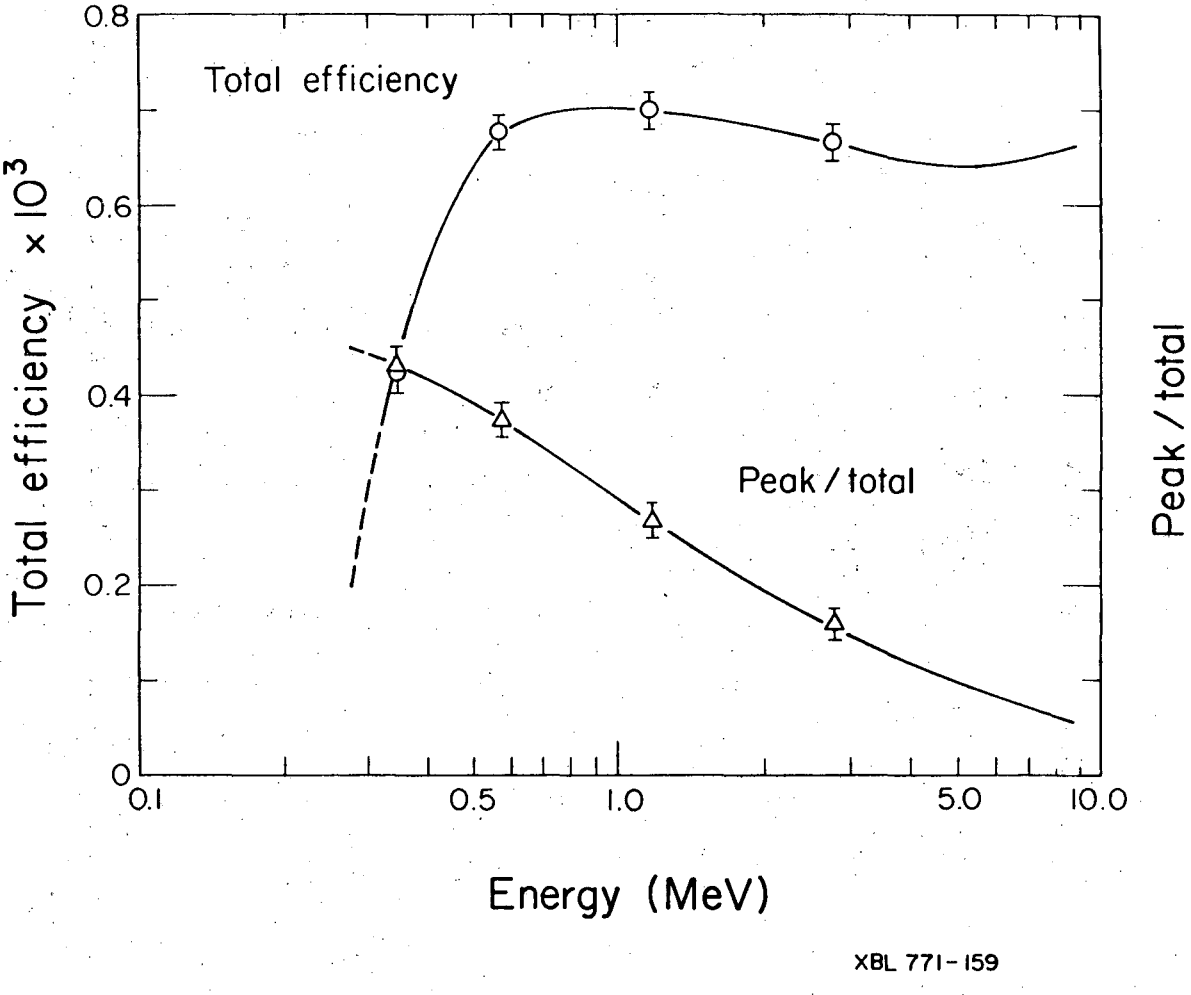

Fig. 4

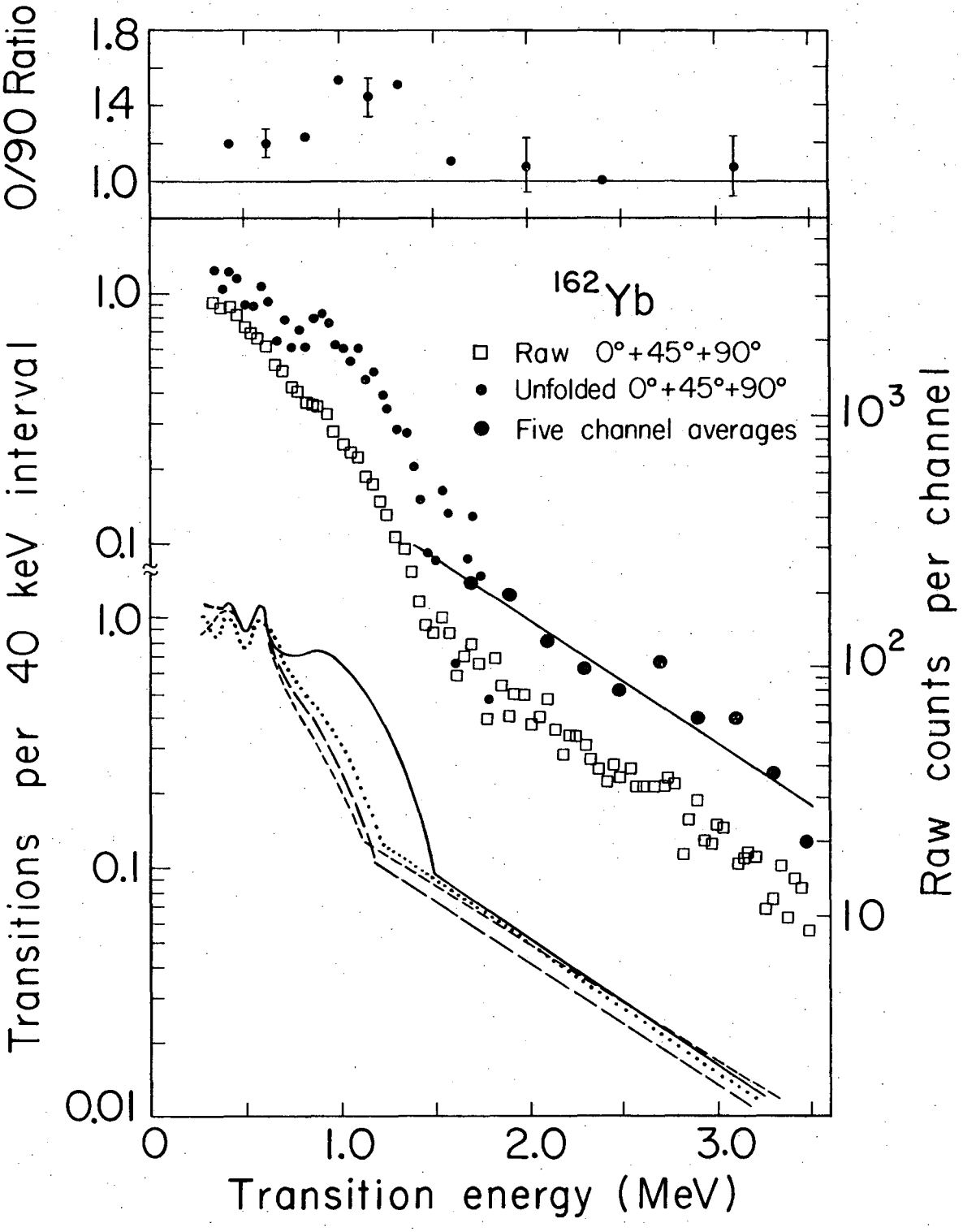

XBL 771-162A

Fig. 5

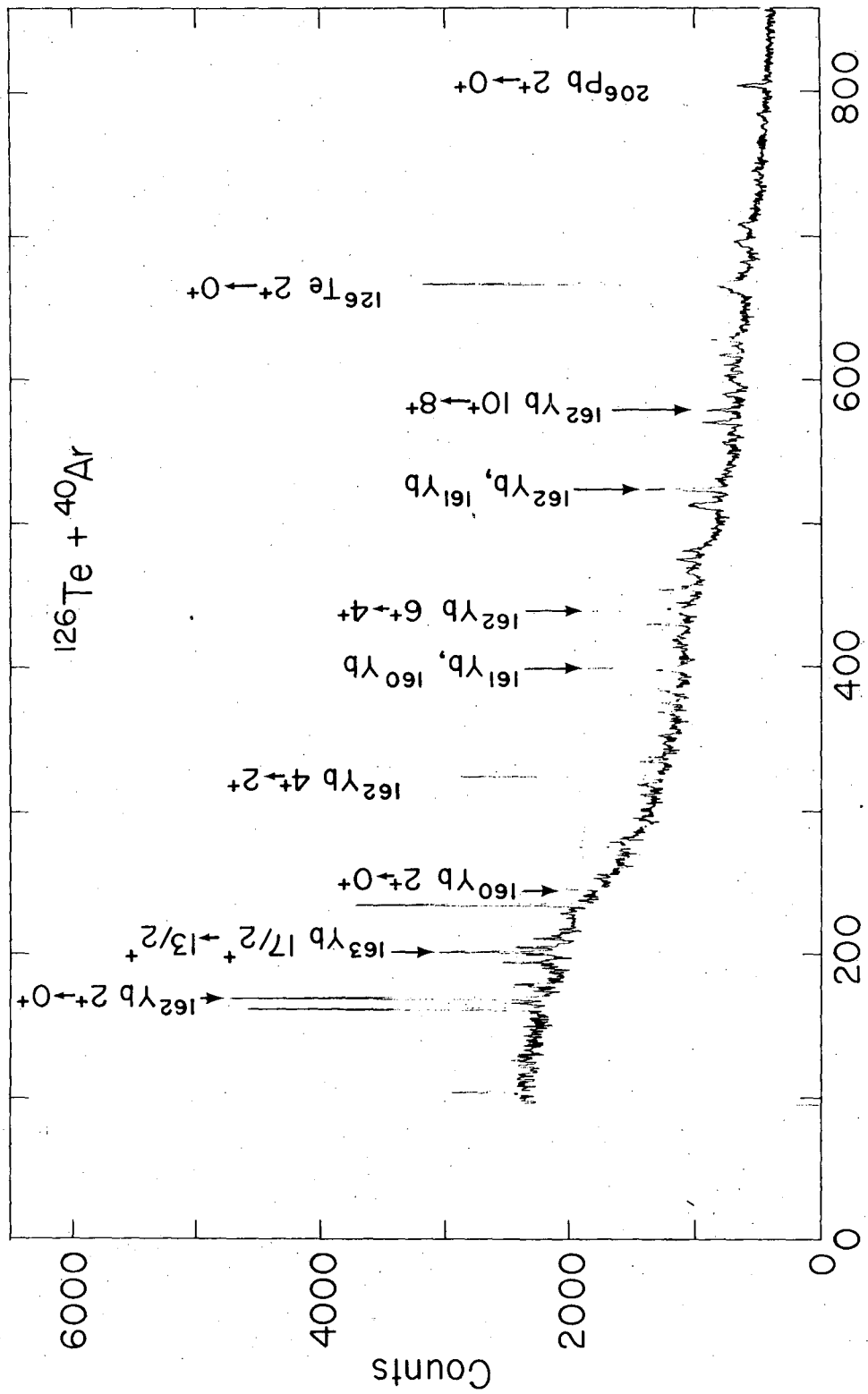

XBL 771-165

Fig. 6

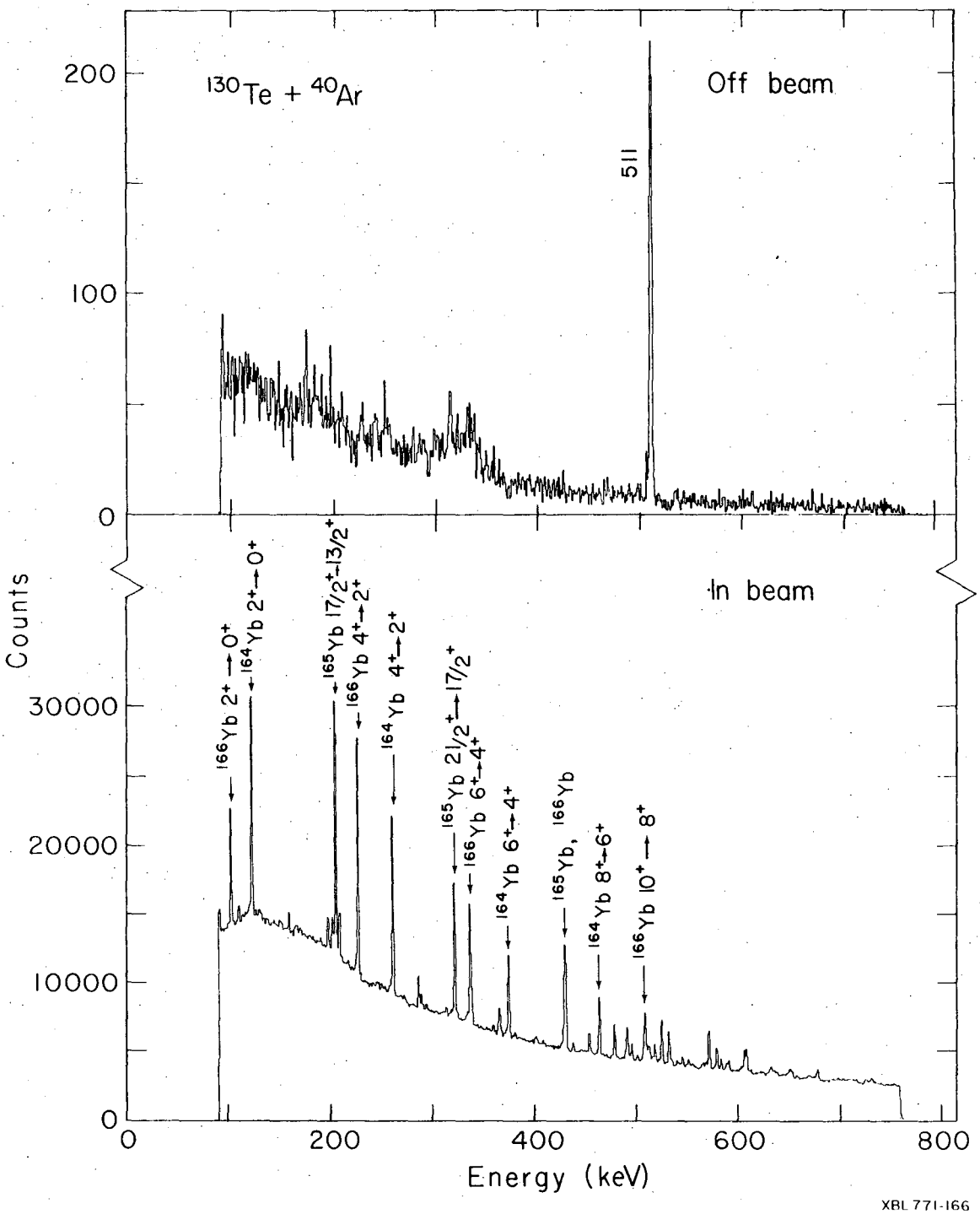
^{130}Te + ^{40}Ar
Off beam
511
In beam
Counts
Energy (keV)
^{166}Yb 2$^+$ → 0$^+$
^{164}Yb 2$^+$ → 0$^+$
^{165}Yb 17/2$^+$→13/2$^+$
^{166}Yb 4$^+$→2$^+$
^{164}Yb 4$^+$→2$^+$
^{165}Yb 21/2$^+$→17/2$^+$
^{166}Yb 6$^+$→4$^+$
^{164}Yb 6$^+$→4$^+$
^{165}Yb, ^{166}Yb
^{164}Yb 8$^+$→6$^+$
^{166}Yb 10$^+$ → 8$^+$
XBL 771-166

Fig. 7

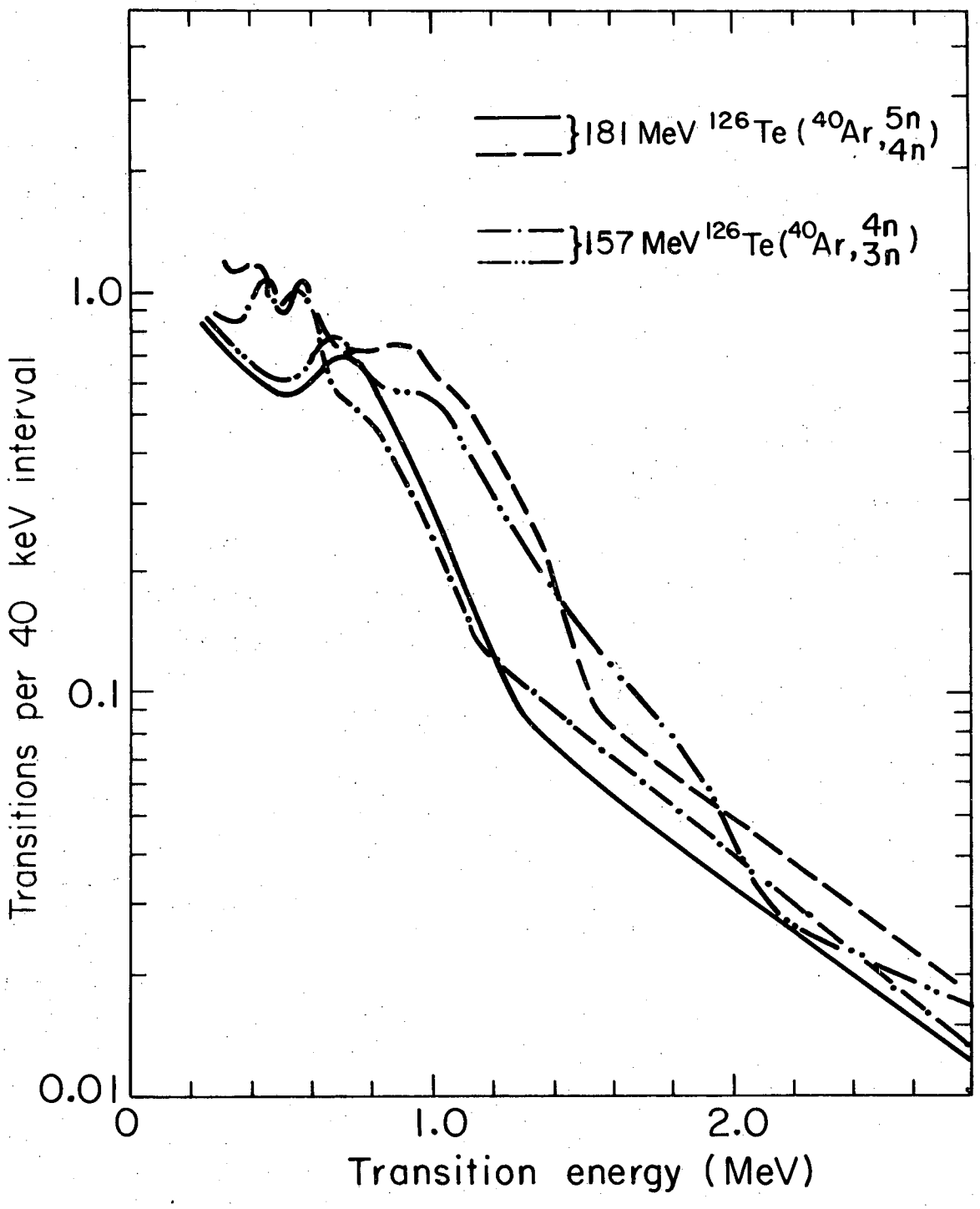

XBL 771-157

Fig. 8

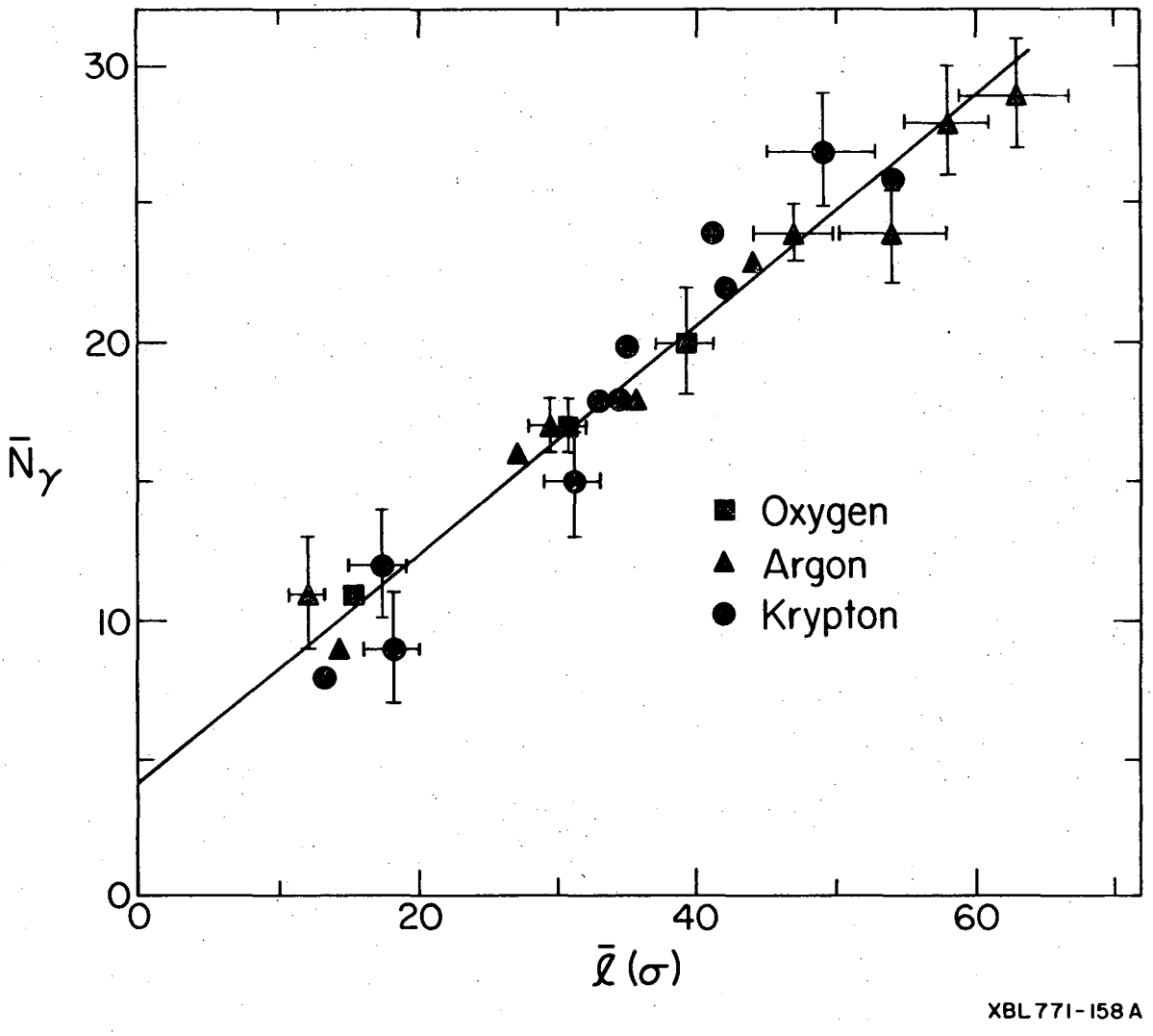
30
20
10
0
0
20
40
60
$\bar{N}_\gamma$
$\bar{\ell}$ (σ)
Oxygen
Argon
Krypton
XBL771-158A

Fig. 9

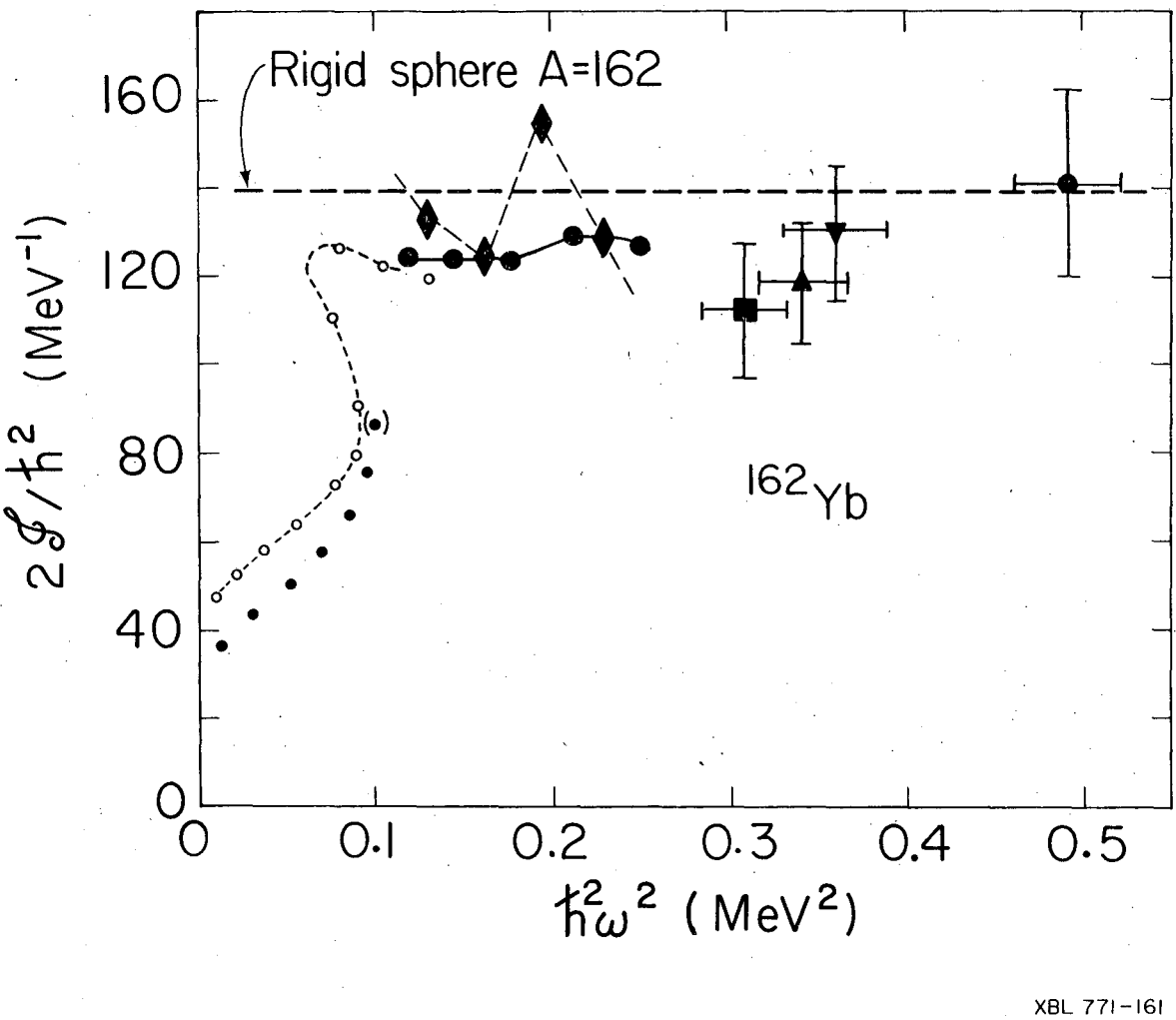

Fig. 10

TECHNICAL INFORMATION DIVISION
LAWRENCE BERKELEY LABORATORY
UNIVERSITY OF CALIFORNIA
BERKELEY, CALIFORNIA 94720